DISCLAIMER

Observation of the dynamics leading to a conical intersection in dissociative electron attachment to water

D. J. Haxton,[1] H. Adaniya,[2,1] D. S. Slaughter,[1] B. Rudek,[1,3] T. Osipov,[1]
T. Weber,[1] T. N. Rescigno,[1] C. W. McCurdy,[1,4] and A. Belkacem[1]

[1]*Lawrence Berkeley National Laboratory, Chemical Sciences, Berkeley, CA 94720, USA*
[2]*Department of Applied Science, University of California, Davis,CA 95616, USA*
[3]*J. W. Goethe Universität, 60438 Frankfurt, Germany*
[4]*Departments of Applied Science and Chemistry, University of California, Davis,CA 95616, USA*

Following prior work on the lower-energy resonances, we apply techniques of momentum imaging and *ab initio* scattering calculations to the process of dissociative electron attachment to water via the highest-energy $^2B_2$ resonance. We focus on the H^- anion fragment, which is produced via dynamics passing through and avoiding the conical intersection with the lower A_1 state, leading to OH ($^2\Pi$) and OH ($^2\Sigma$), respectively. The momentum imaging technique, when combined with theoretical calculations on the attachment amplitude and dissociation dynamics, demonstrates that the angular distributions provide a signature of the location of the conical intersection in the space of nuclear configurations.

PACS numbers: 34.80.Ht

Conical intersections play diverse roles in chemistry, and are one of the main avenues through which the coupling of nuclear and electronic motion proceeds in everyday molecules[1–3]. Dynamics on excited state potential energy curves often involves conical intersections, which are ubiquitous for large molecules and highly excited states. Conical intersections are relevant to a variety of biologically and materially important processes, such as the absorption of light by chromophores [4, 5].

The effect of conical intersections in providing a mechanism for the quenching of excited states has been long established[6–8], and numerous quantitative studies on their effect on branching ratios have been made[9–13]. There are many examples of studies that demonstrate manipulation of conical intersection dynamics, for instance in a pump-probe framework[5, 14, 15]. The measurement of angular distributions may permit the identification of the electronic symmetry or nuclear conformation of the initial state[12, 13, 16, 17], as well as insight into the dissociation dynamics[18–23], in dissociating systems having a conical intersection.

A conical intersection between the $^2B_2$ and $^2A_1$ metastable states of the water anion was predicted [24] and demonstrated to be central to the dynamics following attachment to the $^2B_2$ state [25, 26]. Dissociative electron attachment (DEA) to the H_2O molecule proceeds via these and the $^2B_1$ state at incident electron energies of approximately 12, 8.5 and 6.5 eV respectively, and additionally in the condensed phase via a deep-valence state at approximately 25eV [27]. The negative ion states subsequently fragment to produce the anions H^-, O^- and OH^-, in various arrangements [28–37]. Attachment to the $^2B_2$ state leads to H^- + OH ($^2\Sigma$), avoiding the conical intersection, or H^- + OH ($^2\Pi$), passing through it.

Here, by combining calculations on the molecular-frame attachment amplitude with angular distributions obtained from experiment, we are able to confirm the location of a conical intersection in the space of nuclear geometries. The bending of the molecule to access the conical intersection leaves a clear imprint on the angular distributions for the OH (X $^2\Pi$) + H^- fragment. Our results are consistent with direct dissociation on the $^2B_2$ state, avoiding the conical intersection, and bending by an additional 15 degrees to access the lower OH (X $^2\Pi$) asymptote, going through the conical intersection. The angular distributions are therefore seen to directly reflect the bending dynamics required to transit the conical intersection, and its location relative to the starting angle of 104.5°.

The experimental and theoretical methods employed here parallel those described in our previous publication[38]. In that work we provided a mechanistic study of the dynamics of DEA via the $^2A_1$ state that demonstrated the coupled electronic and nuclear motion inherent to the process. The nuclear dynamics of dissociation was demonstrated to deviate markedly from the axial recoil approximation which provides the zeroth-order description to these dynamics via the analogy to a diatomic, and the angular distributions were well reproduced by the method.

Our experimental approach will be described in detail in a separate paper and therefore only a general outline is presented here. A 50 kHz pulsed electron beam, produced by an electron gun, was directed to the interaction region, defined by the intersection of the electron beam and an effusive water vapor produced by a 0.5 mm - diameter stainless steel capillary directed at an angle of 90° to the electron gun. The electron pulse was typically 80 ns full width at half maximum (FWHM) and the electron energy resolution was found to be 0.8 eV FWHM, measured as twice the energy offset observed in achieving 50% of the peak ion yield at the sharp 6 eV

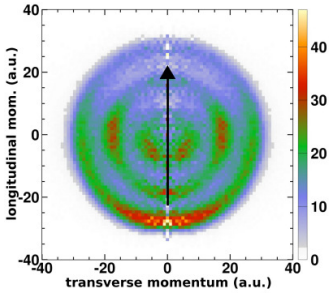

FIG. 1: (Color online) Experimental COLTRIMS image of H^- fragments from attachment at 11.3eV. The transverse and longitudinal momentum in atomic units relative to the incident electron are plotted along the abscissa and ordinate, respectively, with the incident electron traveling bottom (backwards) to top (forwards).

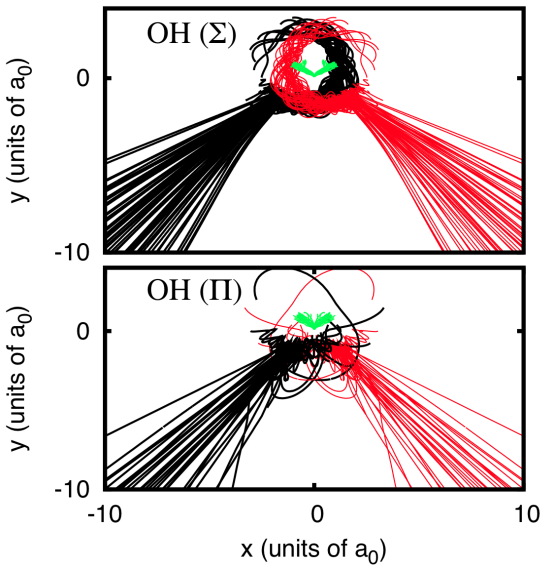

FIG. 2: (Color online) Trajectories leading through (top) and avoiding (bottom) the conical intersection, in the space-fixed frame. The molecule starts at the top of the figure and the paths of the oxygen (light grey; green online; staying near the origin) and two hydrogen atoms (black and dark grey; black and red online) are plotted for an ensemble of trajectories.

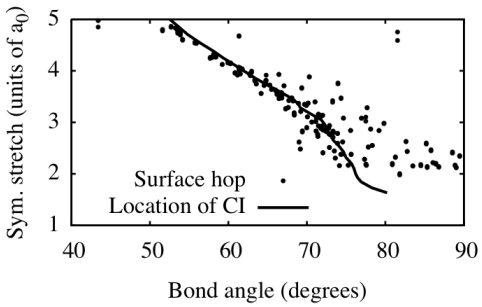

FIG. 3: Location of the $^2B_2$ / $^2A_1$ conical intersection (line), which occurs at equal bond lengths $r_1 = r_2$, and location of surface hops (points) as functions of symmetric stretch coordinate and bond angle.

H^- threshold for DEA to H_2O, compared with the high-resolution ion yield measurements of Fedor et al. [33]. The interaction region was centered between two large parallel electrodes separated by 15 mm. One electrode had a 1 mm aperture to transmit the molecular beam and was pulsed with a negative bias after the electron bunch exited the interaction region, driving negative ions through a grounded mesh in the opposing electrode and into the spectrometer, which was oriented at 90° with respect to the electron beam. Scattered electrons were prevented from entering the spectrometer by a uniform DC magnetic field of typically 25 G, generated by a pair of Helmholtz coils that were oriented coaxially to the electron beam and confined it. The cylindrical spectrometer, based on the COLTRIMS [39] technique, consisted of 27 open copper electrodes with an acceleration region of 25 V/cm, a position-focusing lens, followed by a field-free drift region. The lens focused the 2-D position-image of the finite interaction region onto the detector, while the target spatial extent in the direction of the spectrometer axis was reduced by employing Wiley-McLaren time-focusing [40]. Negative ions were post-accelerated after the spectrometer to typically 500 eV before detection by a position-sensitive delay line detector. The entire spectrometer and detector assembly were housed in an aluminum cylindrical shield to further reduce the scattered electron background. A CAMAC time to digital converter system collected the position and time of flight (TOF) data and the raw data was stored in list mode format for offline analysis.

The ion spectrometer collects the full 4π sphere of dissociating anions while actively discriminating against electrons. Negative ions originating from residual background gas are removed in offline analysis by mass and ion kinetic energy selection. The three-dimensional momentum images of the ionic fragment, determined from the final ion position on the detector and TOF, yield a kinematically complete picture of two-body dissociation and permit the discrimination of three-body breakup events. A typical H^- momentum distribution for the $^2B_2$ resonance is shown in Fig.1. Three distinct rings are clearly resolved, each illustrating a different dissociation pathway leading to different ion momenta. We can clearly determine the internal energy of the OH fragment from the kinetic energy release: the outer-most ring corresponds to the H^- and OH($^2\Pi$), while the second ring is due to H^- and OH($^2\Sigma$) and the inner-most band is the result of 3-body breakup.

In order to make a connection between the lab-frame experimental observations and the dynamics in the body frame, we use a combination of quantum-mechanical cal-

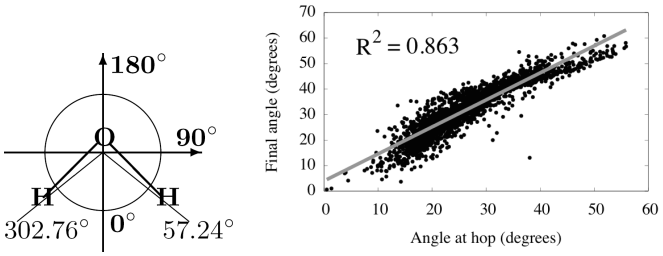

FIG. 4: Left: Definition of molecular frame angles relative to the center of mass. Right: In terms of these angles, there is strong correlation between the direction of the space-fixed momentum vector upon transit through the conical intersection and its final direction. Final recoil as a function of the angle of crossing, black dots; best linear fit, grey line.

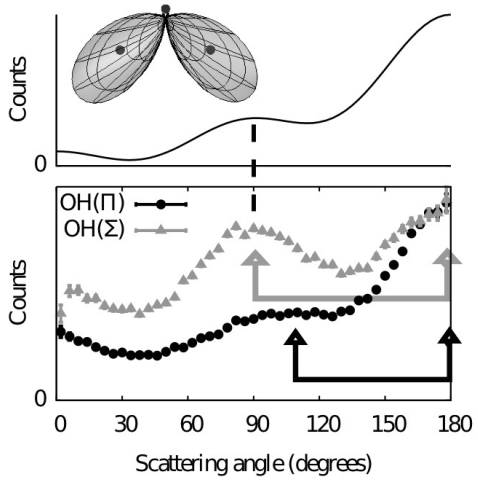

FIG. 5: Top: entrance amplitude V_a as a function of polar angle in the molecular frame, and axial recoil prediction for lab frame H^- angular distribution as a function of scattering angle from the $^2B_2$ resonance. Bottom: Experimental angular distributions of H^- fragments (dots) corresponding to H^- + OH ($^2\Sigma$) (grey triangles) and H^- + OH ($^2\Pi$) (black circles) at 11.3eV. Error bars indicate one standard deviation. The arrows and dashed line are intended to guide the eye and are referred to in the text.

culations of the body-frame attachment amplitude [41] and classical trajectory calculations on complex-valued potential energy surfaces [25]. Autoionization on the complex-valued potential energy surfaces is accounted for stochastically via a survival probability at each timestep, $\exp(-\Gamma(\vec{R})\Delta t)$, where $\Gamma(\vec{R})$ is the width of the resonance in the Born-Oppenheimer approximation. The present calculations employ Tully's fewest switches method[42] to incorporate the effect of the conical intersection between the $^2B_2$ and $^2A_1$ states.

The trajectories shown in Fig. 2 appear to recoil along straight lines in the asymptotic region. They show a clear signature of the effect of the conical intersection upon the angular distribution in the molecular frame. The conical intersection occurs at small bond angles, from approximately 65 to 85 degrees, as shown in figure 3. As a result, the trajectories avoiding the conical intersection to H^- + OH($^2\Sigma$), shown in the top panel of Fig. 2, recoil at an angle of approximately 45° in the molecular frame, whereas those which pass through it, leading to H- + OH ($^2\Pi$), are emitted at approximately 30° degrees, relative to the initial 57.24°.

In Fig. 4 we show the correlation between the molecular frame momentum angle at the transition through the conical intersection and the final angle of recoil, as calculated with the surface hopping method. The correlation between the direction of momentum at the conical intersection crossing and the asymptotic direction is indeed good, with $R^2 = 0.863$, and thus we see that the final recoil angle is a faithful proxy for the angle at which the molecule traverses the conical intersection.

In the bottom panel of Fig. 5 we show the experimental results for the lab frame angular distribution for production of OH ($^2\Sigma$), grey triangles, avoiding the conical intersection, and OH ($^2\Pi$), black dots, passing through the conical intersection. These are determined directly from the ion momentum distribution integrated over each kinetic energy peak corresponding to the bands in Fig. 1 due to two-body dissociation.

We may understand these distributions by examining the probability of electron attachment as a function of angle of incidence in the molecular frame. This probability is the square of the entrance amplitude[43], labeled V_a; $V_a(\theta,\phi;\vec{R}) = \left\langle \Psi^-(\theta,\phi;\vec{R})|H|\varphi \right\rangle$, where Ψ^- is a background scattering state with incident wave at angle θ,ϕ, and φ is a discrete approximation to the resonance state. If ϕ is the azimuthal angle about the recoil axis, and the variation with respect to $\vec{R}$ can be neglected (the constant eigenmode approximation), then the prediction for the observed angular distribution is[43] $\int d\phi\ |V_a(\theta,\phi)|^2$.

In the top panel of Fig. 5 we show the entrance amplitude $V_a(\theta,\phi)$ in the molecular frame at the equilibrium geometry of the neutral and the axial recoil prediction for the angular dependence given this entrance amplitude. The entrance amplitude is peaked along the OH bonds, favoring attachment by electrons incident in these directions. The axial recoil prediction shows two peaks, at approximately 90 and 180° degrees, in the perpendicular and backward directions. With reference to the entrance amplitude in the inset of this figure, these two peaks may be understood as resulting from attachment and dissociation along different and the same OH bonds, respectively.

The experimental results in the bottom panel of Fig. 5 also show two peaks in the angular distribution, marked with grey and black arrows. The dissociation dynamics of this highly excited metastable state are different from

the axial recoil prediction, also shown in Fig. 5. The backwards (180°) peak is suppressed in the experiment; this feature will be discussed in subsequent work.

We focus on the position of the two peaks. The difference in peak locations is highlighted by colored arrows in the bottom of Fig. 5. One can see that the peaks occur farther apart for production of H^- + OH ($^2\Sigma$), avoiding the conical intersection, grey triangles, than for production of H^- + OH ($^2\Pi$), passing through the conical intersection, black dots. For the former, the positions of the peaks at approximately 90 and 180° scattering angle comport with the axial recoil prediction shown in the top panel of Fig 5. As shown by the dashed line in Fig. 5, the perpendicular peak occurs at the same scattering angle as it is predicted to by the axial recoil approximation. This similarity between the axial recoil prediction and the experimental results for OH ($^2\Sigma$) is consistent with dissociation in which the bond angle changes relatively little, tending to avoid the conical intersection. For OH ($^2\Pi$), black dots, passing through the conical intersection, the bond angle must decrease and as a consequence the perpendicular peak is shifted backwards and the backwards peak is shifted forward somewhat by this scissoring motion concomitant with dissociation and passage through the conical intersection. The classical trajectory calculations indicate that the observed recoil angle does indeed reflect the angle of passage through the conical intersection and therefore eliminate the possibility that the observed differences are due to different dynamics beyond the range of the conical intersection. Therefore, the experimental results corroborate the position of the conical intersection, occurring at small bond angles relative to the 104.5° starting point, calculated in Ref. [25].

In conclusion, we have demonstrated that the observed variations in the final state angular dependence for H^- production via dissociative attachment to the $^2B_2$ Feshbach resonance of the water anion are a clear signature of the dynamics either passing through or avoiding the conical intersection. This conical intersection lies at small bond angles and is imaged via the closing of the angle between of the two peaks seen in the experimental angular distributions. The use of molecular-frame calculations on the attachment probability permits this connection between the observed features and the dynamics of dissociation.

This work was performed under the auspices of the US DOE by LBNL under Contract DE-AC02-05CH11231 and was supported by the U.S. DOE Office of Basic Energy Sciences, Division of Chemical Sciences.

[1] D. Yarkony, Rev. Mod. Phys. **68**, 985 (1996).
[2] M. Baer, Physics Reports **358**, 75 (2002).
[3] G. A. Worth, Annual Review of Physical Chemistry **55**, 127 (2004).
[4] A. Virshup, C. Punwong, T. Pogorelov, B. A. Lindquist, C. Ko, and T. Martinez, J. Phys. Chem. B **113**, 3280 (2009).
[5] S. Logunov, V. Volkov, M. Braun, and M. El-Sayed, Proceedings of the National Academy of Sciences of the United States of America **98**, 8475 (2001).
[6] H. Krautwld, L. Schneider, K. Welge, and M. Ashfold, Faraday Discuss. Chem. Soc. **82**, 99 (1986).
[7] T. Martinez, Chem. Phys. Lett. **272**, 139 (1997).
[8] S. Harich, X. Yang, X. Yang, and R. Dixon, Phys. Rev. Lett. **87**, 253201 (2001).
[9] M. Abe, Y. Ohtsuki, Y. Fujimura, Z. Lan, and W. Domcke, J. Chem. Phys **124**, 224316 (2006).
[10] A. Hoffmann and R. de Vivie-Riedle, J. Chem. Phys. **112**, 5054 (2000).
[11] B. C. Hoffman and D. R. Yarkony, J. Chem. Phys. **113**, 10091 (2000).
[12] G. Waschewsky, P. Kash, T. Myers, D. Kitchen, and L. Butler, J. Chem. Soc. Faraday Trans. **90**, 1581 (1994).
[13] A. Eppink and D. Parker, J. Chem. Phys. **109**, 4758 (1998).
[14] H. Kang, B. Jung, and S. Kim, J. Chem. Phys. **118**, 6717 (2003).
[15] L. Seidner, G. Stock, A. Sobolewski, and W. Domcke, J. Chem. Phys. **96**, 5298 (1992).
[16] W. McGivern, R. Li, P. Zou, and S. North, J. Chem. Phys. **111**, 5771 (1999).
[17] P. Kash, G. Waschewsky, R. Morss, L. Butler, and M. Franci, J. Chem. Phys. **100**, 3463 (1994).
[18] G. Amaral, K. Xu, and J. Zhang, J. Chem. Phys. **114**, 5164 (2001).
[19] G. Waschewsky, D. Kitchen, P. Browning, and L. Butler, J. Phys. Chem. **99**, 2635 (1995).
[20] J. Wei, A. Kuczmann, J. Reidel, F. Renth, and F. Temps, Phys. Chem. Chem. Phys. **5**, 315 (2005).
[21] D. Mordaunt, M. Ashfold, and R. Dixon, J. Chem. Phys. **109**, 7659 (1998).
[22] J. Liu, F. Wang, H. Wang, B. Jiang, and X. Yang, J. Chem. Phys. **122**, 104309 (2005).
[23] S. Harich, X. Yang, D. Hwang, J. Lin, X. Yang, and R. Dixon, J. Chem. Phys. **114**, 7830 (2001).
[24] D. J. Haxton, T. N. Rescigno, and C. W. McCurdy, Phys. Rev. A **72**, 022705 (2005).
[25] D. J. Haxton, C. W. McCurdy, and T. N. Rescigno, Phys. Rev. A **75**, 012710 (2007).
[26] D. J. Haxton, T. N. Rescigno, and C. W. McCurdy, Phys. Rev. A **75**, 012711 (2007).
[27] G. A. Kimmel and T. M. Orlando, Phys. Rev. Lett. **77**, 3983 (1996).
[28] N. B. Ram, V. S. Prabhudesai, and E. Krishnakumar, J. Phys. B **42**, 225203 (2009).
[29] P. Rawat, V. S. Prabhudesai, G. Aravind, N. Bhargavaram, M. A. Rahman, and E. Krishnakumar, Journal of Physics: Conference Series **80**, 012018 (2007).
[30] P. Rawat, V. S. Prabhudesai, G. Aravind, M. A. Rahman, and E. Krishnakumar, J. Phys. B **40**, 4625 (2007).
[31] E. Krishnakumar, V. S. Prabhudesai, and N. B. Ram, Journal of Physics: Conf. Series **88**, 012073 (2007).
[32] V. S. Prabhudesai, D. Nandi, and E. Krishnakumar, J. Phys. B **39**, 277 (2006).
[33] J. Fedor, P. Cicman, B. Coupier, S. Feil, M. Winkler, K. Gluch, J. Husarik, D. Jaksch, B. Farizon, N. J. Mason, et al., J. Phys. B **39**, 3935 (2006).

[34] D. S. Belic, M. Landau, and R. H. Hall, J. Phys. B. **14**, 175 (1981).
[35] R. N. Compton and L. G. Christophorou, Phys. Rev. **154**, 110 (1967).
[36] C. E. Melton, J. Chem. Phys. **57**, 4218 (1972).
[37] D. J. Haxton, T. Rescigno, and C. W. McCurdy, Phys. Rev. A **78**, 040702 (2008).
[38] H. Adaniya, Phys. Rev. Lett. **103**, 233201 (2009).
[39] R. Dörner, et al., Phys. Rep. **330**, 96 (2000).
[40] W. C. Wiley and I. H. McLaren, Rev. Sci. Inst. **26**, 1150 (1955).
[41] D. J. Haxton, C. W. McCurdy, and T. N. Rescigno, Phys. Rev. A **73**, 062724 (2006).
[42] J. Tully, J. Chem. Phys. **93**, 1061 (1990).
[43] T. F. O'Malley and H. S. Taylor, Phys. Rev. **176**, 207 (1968).